**IN FOCUS**

# Single vs. swarm detection of microparticles and exosomes by flow cytometry

E. VAN DER POL,*† M. J. C. VAN GEMERT,† A. STURK,* R. NIEUWLAND* and T. G. VAN LEEUWEN†‡

*Laboratory of Experimental Clinical Chemistry and †Biomedical Engineering and Physics, Academic Medical Center, University of Amsterdam, Amsterdam; and ‡Biomedical Photonic Imaging, University of Twente, Enschede, the Netherlands*

**Summary.** *Background:* Microparticles and exosomes are cell-derived vesicles and potential biomarkers for disease. Recently, the Scientific Standardization Committee collaborative workshop of the ISTH initiated standardization of vesicle detection by flow cytometry with polystyrene beads. Because polystyrene beads have different optical properties from biological vesicles, and because the mechanisms causing the detection signal are incompletely understood, there are contradictions between expected and observed results. *Objectives:* To develop a model with which to relate the detection signal of a flow cytometer to the diameter of vesicles and clarify observed discrepancies. *Methods:* We combined measurements of polystyrene and silica beads with an estimated refractive index of vesicles and performed Mie calculations of light scattering. *Results:* We established the relationship between measured light scattering and the diameter of vesicles. The Megamix gating strategy proposed by the Scientific Standardization Committee selects single vesicles and cells with diameters between 800 and 2400 nm when applied on the forward-scattering detector of regular flow cytometers. Nevertheless, we demonstrated that, irrespective of the applied gating, multiple vesicles smaller than 220 nm or multiple 89-nm silica beads were counted as a single event signal at sufficiently high concentrations. *Conclusions:* Vesicle detection by flow cytometry is attributed to large single vesicles and swarm detection of smaller vesicles; that is, multiple vesicles are simultaneously illuminated by the laser beam and counted as a single event signal. Swarm detection allows the detection of smaller vesicles than previously thought possible, and explains the finding that flow cytometry underestimates the concentration of vesicles.

Correspondence: Edwin van der Pol, Academic Medical Center, University of Amsterdam, Biomedical Engineering and Physics, Meibergdreef 9, 1105 AZ Amsterdam, the Netherlands.
Tel.: + 31 20 5664386; fax: + 31 20 6917233.
E-mail: e.vanderpol@amc.uva.nl

## Introduction

Microparticles and exosomes are cell-derived vesicles present in body fluids that contribute to coagulation, inflammation, cellular homeostasis and survival, intercellular communication, and transport of waste materials [1–3]. The size, concentration, biochemical composition and cellular origin of these biological vesicles contain clinically relevant information [4–6]. However, because of the small size of vesicles (30 nm to 1 μm), they are below the detection range of many currently used techniques [7]. Throughout this article, we will use 'vesicles' as a generic term for all types of extracellular, biological vesicle.

Approximately 75% of laboratories apply flow cytometry to detect vesicles in clinical samples [8]. A flow cytometer guides cells and vesicles through a laser beam in a hydrodynamically focused fluid stream. One detector is placed in line with the laser beam, and measures the forward-scattered light (FSC). Other detectors measure the side-scattered light (SSC) and fluorescence intensity perpendicular to the beam. Light scattering by vesicles is essential, as scattering is generally used as the trigger signal telling the instrument that a vesicle is present.

A difficulty with flow cytometry is that the relationship between the measured light scattering and the diameter of vesicles is unknown, resulting in recent discussions about the standardization of vesicle detection [9–11] and in unexplained contradictions between the expected and observed measurement results. For example, according to the literature, the smallest polystyrene beads that can be detected by commercial flow cytometers typically have a diameter between 200 nm and 300 nm [9,12,13]. Because vesicles have a lower refractive index than polystyrene beads, they scatter light approximately 10-fold less efficiently than polystyrene beads [9]. Consequently, the smallest single vesicles that are detectable by flow cytometry must be larger than ~ 500 nm. Using transmission electron microscopy (TEM) image analysis, we have recently

shown that urinary vesicles are smaller than 500 nm [7], so we would not expect these vesicles to be detected by flow cytometry. Nevertheless, urinary vesicles are detectable by flow cytometry [14], although, from reference measurements with nanoparticle tracking analysis and atomic force microscopy, we now know that flow cytometry underestimates the concentration of vesicles by $\sim$ 1000-fold [15,16].

To resolve the contradictions in vesicle detection by flow cytometry, we will first present measurements on polystyrene beads and silica beads of known diameter, concentration, and refractive index. Combined with Mie calculations of the optical scattering power, this allows calibration of the flow cytometer, i.e. relating the detected scattering power to the diameter of single polystyrene or silica beads. On that basis, and using an estimated refractive index, we assess the diameter range of the smallest detectable single vesicles. In addition, we show that 89-nm silica beads, which have optical properties resembling those of vesicles, can be detected by regular flow cytometry, albeit at a higher concentration than used to detect single beads. Using dilution series of silica beads and cell-free urine, we elucidate the underlying mechanisms of vesicle detection.

## Methods

### Samples

***Beads*** Table 1 summarizes the mean diameter and standard deviation of the used NIST-traceable polystyrene beads (Thermo Fisher Scientific, Waltham, MA, USA) and silica beads (Kisker Biotech, Steinfurt, Germany). At the illumination wavelength of our flow cytometer, which is 488 nm, the refractive indexes of polystyrene and silica are 1.605 and 1.445, respectively. For comparison, the refractive index of water is 1.337 at this wavelength. As the refractive index of vesicles is assumed to be 1.38 inside the vesicle and 1.48 at the 10-nm-thick phospholipid membrane [17–20], the optical

**Table 1** Diameter of polystyrene beads and silica beads and the efficiency with which single beads are detected by flow cytometry

| Material | Diameter (nm) | Detection efficiency |
|---|---|---|
| Polystyrene | 102 $\pm$ 5 | 0 |
| | 203 $\pm$ 5 | 0.9 $\pm$ 0.2 |
| | 400 $\pm$ 7 | 1.0 $\pm$ 0.2 |
| | 596 $\pm$ 8 | 0.9 $\pm$ 0.2 |
| | 799 $\pm$ 5 | 1.0 $\pm$ 0.1 |
| | 994 $\pm$ 10 | 1.0 $\pm$ 0.1 |
| | 3005 $\pm$ 30 | 1.2 $\pm$ 0.2 |
| Silica | 89 $\pm$ 36 | 0 |
| | 204 $\pm$ 35 | 0.6 $\pm$ 0.2 |
| | 389 $\pm$ 75 | 1.1 $\pm$ 0.3 |
| | 610 $\pm$ 101 | 1.0 $\pm$ 0.2 |
| | 732 $\pm$ 107 | 1.0 $\pm$ 0.2 |
| | 988 $\pm$ 132 | 1.2 $\pm$ 0.3 |
| | 2795 $\pm$ 472 | 1.1 $\pm$ 0.4 |

Diameter is expressed as mean $\pm$ standard deviation. The detection efficiency is defined as the ratio between the concentration as determined by the flow cytometer and the prepared concentration.

properties of silica beads resemble those of vesicles better than those of polystyrene beads. To explore the detection limit of our flow cytometer (Figs 4 and 5), beads were diluted in purified and deionized water (MilliPore, Billerica, MA, USA) to a concentration of $10^5$ mL$^{-1}$. For this concentration, the expected count rate is 100 events s$^{-1}$ at an estimated flow rate of 60 μL min$^{-1}$, which is within the recommended count rate for the flow cytometer. To explore the underlying mechanisms of vesicle detection (Fig. 6), dilution series of silica beads were prepared, in which the ratio of 89-nm and 610-nm silica beads was varied.

***Vesicles*** Cell-derived vesicles from human urine were used as a reference sample, because vesicles can be easily isolated without substantial contamination [7]. Fresh morning urine from five overnight-fasting healthy male subjects was collected, pooled, and centrifuged in 50-mL Falcon tubes for 10 min at 180 $\times$ g and 4 °C (MIKRO 200 R; Hettich, Tuttlingen, Germany) within 10 min after collection. The supernatant (45 mL) was collected and centrifuged for another 20 min at 1550 $\times$ g and 4 °C to remove the remaining cells. Aliquots of the supernatant (40 mL) were frozen in liquid nitrogen and stored at − 80 °C. Samples were thawed on melting ice for 1 h, and centrifuged for 10 min at 1550 $\times$ g and 4 °C to remove precipitated amorphous salts.

### TEM

For TEM analysis, vesicles were isolated by ultracentrifugation (60 min at 154 000 $\times$ g and 4 °C), and washed once in phosphate-buffered saline (PBS)–citrate. Next, vesicles were resuspended in 0.2% paraformaldehyde (w/v). After fixation for 24 h, vesicles were allowed to adhere to formvar-carbon coated 300 mesh grids (Electron Microscopy Sciences, Hatfield, PA, USA), stained with 1.75% uranyl acetate (w/v), and imaged with a transmission electron microscope (CM-10; Philips, Eindhoven, The Netherlands) at 100 kV. From 1000 vesicles, the surface area was determined by use of a custom-made Javascript with the Quick selection tool of PHOTOSHOP version 11.0.2 (Adobe Systems, San Jose, CA, USA). From the surface area, the diameter of each vesicle was calculated to create a size distribution.

### Flow cytometry

FSC and SSC powers were measured for 1 min with a FACSCalibur (Becton Dickinson, Franklin Lakes, NJ, USA) at a high flow rate (60 μL min$^{-1}$). The flow cytometer has a linearly polarized 15-mW argon-ion laser emitting at 488 nm. The beam is elliptically focused to a cross-sectional area of 22 $\times$ 66 μm$^2$, and at high flow rate the sample core diameter is 56 μm [21]. Consequently, the effective beam volume is 22 $\times$ $\pi$ $\times$ 28$^2$ = 5.4 $\times$ 10$^4$ μm$^3$ or 54 pL. The illumination intensity is $\sim$ 1.4 $\times$ 10$^7$ W m$^{-2}$ [22]. We selected SSC as the trigger signal to indicate to the instrument that a vesicle or bead is present. The following detector settings were used

throughout this experiment. For SSC, the applied voltage was 400 V, the gain was 1, and the threshold was 0. For FSC, the amplification was 100, the gain was 1, and the threshold was 0. As no threshold was applied, optical, electronic and fluidic noise contribute to a considerable noise background [23]. However, in modern flow cytometers, both the dark current and stray light are electronically subtracted from the signal coming from the detector by the baseline restorer, resulting in a stable and relatively low noise background of < 10 000 counts min$^{-1}$ in our case. To account for this remaining noise background, a background measurement was performed with purified and deionized water before and after each measurement series. The average SSC and FSC histograms of these background measurements were subtracted from each dataset.

### Mie theory

The power of light scattered in a particular direction by a spherical particle, such as a bead or a vesicle, is calculated by Mie theory, and involves the diameter and refractive index of the particle, the refractive index of the surrounding medium, and the wavelength, polarization and intensity of light [24]. We selected Mie theory because, in contrast to Rayleigh scattering and Faunhofer diffraction, it is valid for any ratio of the diameter of the particle to the wavelength [7,24]. All Mie calculations in this manuscript are based on the MATLAB scripts of Mätzler [25], and are similar to the calculations of Fattaccioli *et al.* [26], but other free software is online available [27]. Data processing was performed with MATLAB (v.7.9.0.529), and graphs were plotted with ORIGINPRO (v.8.0724). As input for the Mie calculations, we used the parameters listed in Table 2. Here, we assumed that urine has a refractive index equal to that of water, and that vesicles are spherical and have refractive indexes of 1.38 ± 0.02 inside and 1.48 at the 10-nm-thick phospholipid membrane [17–20]. Our estimation of the inner

**Table 2** Parameters used for Mie calculations. The refractive indices are provided for room temperature, atmospheric pressure, and an illumination wavelength of 488 nm

| Parameter | Value |
| --- | --- |
| Refractive index: polystyrene | 1.605 |
| Refractive index: silica | 1.445 |
| Refractive index: water | 1.337 |
| Refractive index: vesicle inside | 1.38 ± 0.02 |
| Refractive index: vesicle at the membrane | 1.48 |
| Vesicle membrane thickness (nm) | 10 |
| Illumination wavelength (nm) | 488 |
| Illumination intensity (W m$^{-2}$) | 1.4 × 10$^7$ |
| Collection angle: FSC Becton-Dickinson FACSCalibur (°) | 0.5–7 |
| Collection angle: SSC Becton-Dickinson FACSCalibur (°) | 47–133 |
| Collection angle: FSC Apogee A40 (°) | 1–70 |
| Collection angle: FSC Beckman-Coulter FC500 (°) | 2–16 |

FSC, forward-scattered light; SSC, side-scattered light.

refractive index of vesicles is based on the measured inner refractive index of cells and bacteria [17]. As vesicles originate from their parent cell, we expected that vesicles would have an inner refractive index equal to that of their parent cell.

### Flow cytometer calibration

Flow cytometry provides the detected scattering power in arbitrary units, implying that the relationship between the detected scattering power and the diameter of vesicles is unknown, as illustrated in Fig. 1A. To establish this relationship, we measured the relative power in arbitrary units (a.u.) and, in parallel, calculated the absolute power (mW) of light that scattered by beads of known diameter and refractive index in the direction of the detectors. Figure 1B shows that this approach enables us to obtain a calibration factor that relates
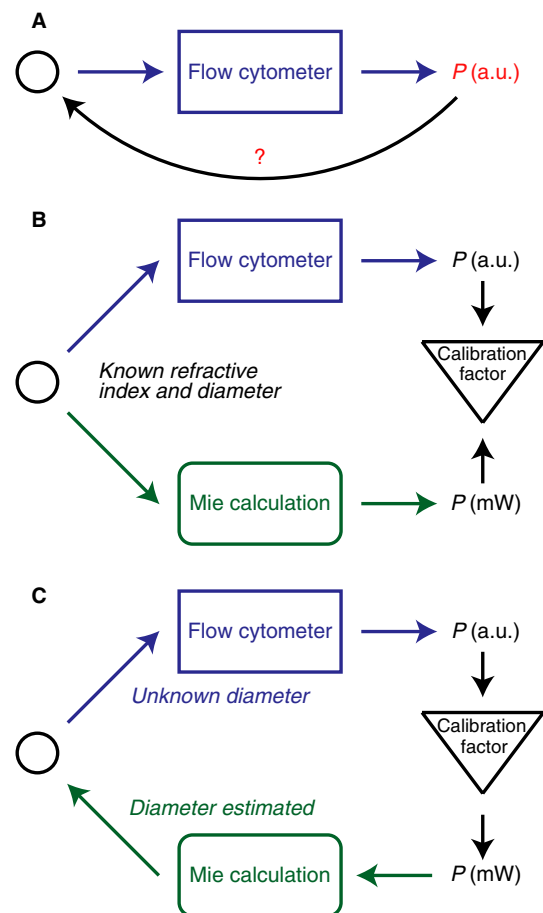


**Fig. 1.** From detected scattering power to vesicle diameter. (A) The relationship between the vesicle (circle) diameter and the detected scattering power *P* in arbitrary units (a.u.) is unknown. (B) From beads (circle) with known diameter and refractive index, the scattering power *P* (a.u.) can be measured. In parallel, the true scattering power *P* (mW) can be calculated by Mie theory to obtain the calibration factor, which relates the detected scattering power to the calculated scattering power. (C) By use of the calibration factor, it is possible to convert the detected scattering power of any spherical particle to the scattering power and apply Mie calculations to estimate the particle diameter.

the detected to the calculated scattering power. The calibration factor is thus a property of the detector and the optical configuration of the instrument, and is independent of the sample. Figure 1C shows that this calibration factor allows estimation of the true diameter of the particle. Note that the calculated scattering power depends on the estimated illumination intensity (Table 2). However, as the detected scattering power is fitted to the calculated scattering power by use of the calibration factor, the relationship between the detected scattering power and the diameter of vesicles remains similar for any value of the illumination intensity.

### Resistive pulse sensing

To estimate the concentration of vesicles in cell-free urine, resistive pulse sensing (Izon qNano, Christchurch, New Zealand) was applied. The thawed cell-free urine was diluted 1 : 10 with PBS. At least 1000 vesicles were counted at a pressure of 6.9 mbar, using both NP100A and NP400A nanopores, which are optimized for the detection of particles with diameters ranging from 50 nm to 200 nm and 200 nm to 800 nm, respectively.

## Results

### Flow cytometry detects vesicles smaller than 220 nm

Figure 2A shows a TEM image of vesicles from urine and Fig. 2B their determined size distribution. The largest vesicles had a diameter of 295 nm. As the diameter of the smallest polystyrene beads that can be detected by commercial flow cytometers is typically between 200 nm and 300 nm [9,12,13], and because vesicles have a lower refractive index than polystyrene beads, we would not expect these urinary vesicles to be detected by flow cytometry.

Figure 3A,B shows the FSC and SSC histograms of the same urine sample measured with flow cytometry. Both histograms show a peak, indicating that vesicles were detected. To exclude the possibility that vesicles larger than 300 nm were present, urine was subsequently filtered with a 220-nm filter

(MilliPore) before analysis. Figure 3C,D shows that, after filtration, FSC and SSC histograms of vesicles were still obtained, although at fewer counts per minute than with the unfiltered sample. Thus, in contrast to our expectations, flow cytometry detected vesicles smaller than 220 nm.

### Scattering power of beads

Figure 4A,C shows FSC histograms of polystyrene beads and silica beads, respectively. The distributions of beads with a diameter smaller than 1000 nm are broad and overlapping. Thus, FSC was unable to resolve the diameter of particles smaller than 1000 nm. Figure 4B,D shows the SSC histograms of polystyrene beads and silica beads, respectively. As the SSC distribution of light scattered by beads was narrow, they could be distinguished from each other. Thus, for our flow cytometer, SSC is more suitable than FSC for resolving particles with a diameter smaller than 1000 nm. As the 102-nm polystyrene beads and the 89-nm silica beads could not be detected, the smallest detectable polystyrene beads and silica beads were 203 and 204 nm, respectively. However, not all 204-nm silica beads were detected. As the flow rate was known, the bead concentration could be calculated and compared with the true concentration. The ratio between the measured and the true concentration is defined as the detection efficiency. For the 204-nm silica beads, the detection efficiency was $0.6 \pm 0.2$. Table 1 shows that the detection efficiency of all other beads was close to 1, meaning that single polystyrene beads and silica beads with diameters of 203 and 389 nm, and larger, could be detected.

### Smallest detectable single vesicles

To establish the relationship between the detected scattering power and the diameter of vesicles, the flow cytometer needs to be calibrated, as shown in Fig. 1. Therefore, the histograms from beads in Fig. 4 were fitted with a normal distribution to determine the mean scattering power and standard deviation for each bead diameter. The detected scattering power is provided in arbitrary units, and is proportional to the absolute
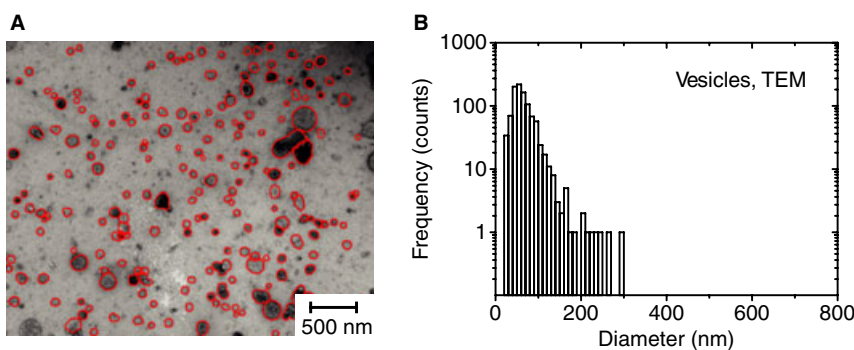


**Fig. 2.** Vesicle detection by transmission electron microscopy (TEM). (A) TEM image of urinary vesicles. The red circles indicate the surface areas of spherical objects. (B) Size distribution (logarithmic vertical scale) of 1000 vesicles determined from five TEM images. The plot shows a distribution with vesicle diameters between 25 nm and 295 nm, with a single peak at 55 nm.
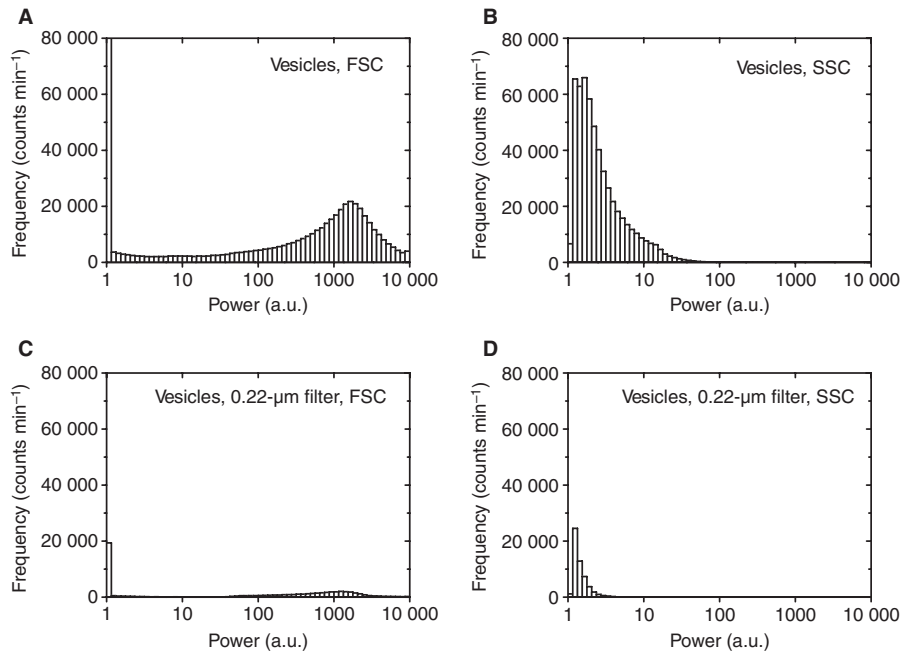
**Fig. 3.** Vesicle detection by flow cytometry. (A) Forward-scattered light (FSC) histogram (logarithmic horizontal scale) of urinary vesicles. A flat peak is observed. In total, $5.5 \times 10^5$ events were counted during 1 min. (B) Side-scattered light (SSC) histogram of urinary vesicles. A single peak is observed. (C) FSC histogram of urinary vesicles filtered through a 220-nm filter. A flat peak is observed. In total, $5.7 \times 10^4$ events were counted during 1 min. (D) SSC histogram of urinary vesicles filtered through a 220-nm filter. A single peak is observed. a.u., arbitrary units.
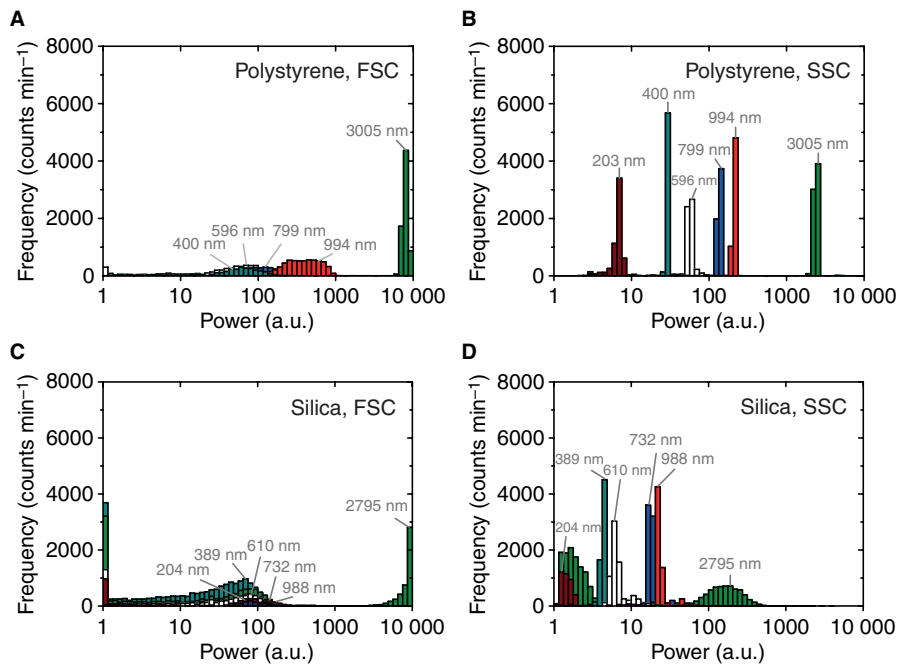


**Fig. 4.** Forward-scattered light (FSC) and side-scattered light (SSC) histograms (logarithmic horizontal scale) for polystyrene beads (A, B) and silica beads (C, D) of known diameters and at a concentration $1 \times 10^5$ mL$^{-1}$. The FSC distributions from beads with a diameter smaller than 1000 nm are broad and overlapping, whereas the SSC distributions for the same beads are narrow and can be distinguished from each other. a.u., arbitrary units.

scattering power (mW), which was calculated by Mie theory. For our instrument, the calibration factors that relate the measured to the calculated scattering power are $2.07 \times 10^{-5}$ for the FSC detector and $1.26 \times 10^{-6}$ for the SSC detector.

Figure 5A shows the measured and calculated FSC power vs. the diameter of polystyrene beads and silica beads. Data points corresponding to a power higher than $1.7 \times 10^{-3}$ mW are in agreement with the Mie calculations. Some beads from which
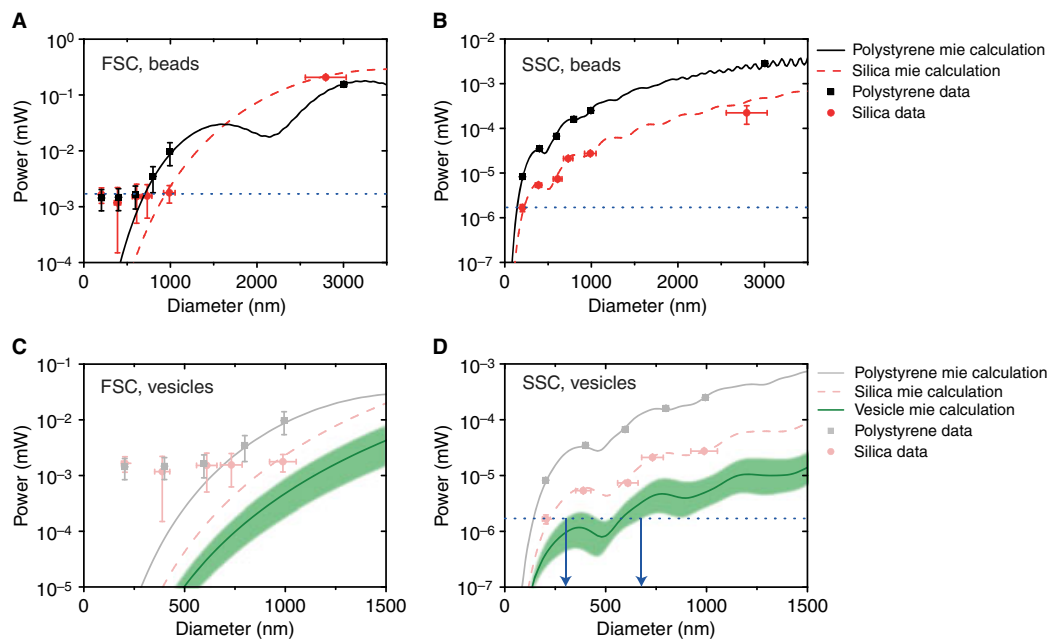
**Fig. 5.** Relationship between the measured light-scattering power of beads and the diameter of vesicles. (A) Measured (symbols) and calculated (lines) forward-scattered light (FSC) power (logarithmic scale) vs. diameter for polystyrene beads (black) and silica beads (red). Data points corresponding to a power higher than $1.7 \times 10^{-3}$ mW (dotted blue line) are in agreement with theory. The trough at 2140 nm for the calculation of polystyrene beads is caused by a Mie resonance. (B) Measured and calculated side-scattered light (SSC) power vs. diameter for polystyrene beads and silica beads. The power increases with increasing particle diameter and refractive index. The detection limit is $1.7 \times 10^{-6}$ mW (dotted blue line). (C) Measured and calculated FSC power vs. diameter for polystyrene beads (gray), silica beads (transparent red), and vesicles (green). The light green area around the Mie calculation for vesicles is a calculated confidence interval, which is based on an assumed inner refractive index of biological vesicles of $1.38 \pm 0.02$. The FSC power increases with increasing particle diameter, and is lower for vesicles than for beads. (D) Measured and calculated SSC power vs. diameter for polystyrene beads, silica beads, and vesicles. The intersection of the detection limit with the Mie calculation for vesicles gives the range of smallest single vesicles that can be detected by the FACSCalibur (blue dotted line), which is 300–700 nm. The calculation parameters are listed in Table 2.

the scattered power was below $1.7 \times 10^{-3}$ mW were detected by FSC, but the observed power was not related to the size of the beads. Figure 5B shows the measured and calculated SSC power vs. diameter for polystyrene beads and silica beads. The power increased with increasing particle diameter and refractive index. The data are in excellent agreement with the Mie calculations, except for the 2795-nm silica beads. We attribute the underestimation of the scattered power of 2795-nm silica beads to a decreased refractive index resulting from porosity, as stated by the manufacturer. The effective refractive index of the porous 2795-nm silica beads that matches with our measurement is 1.423 rather than 1.445. The power corresponding to the smallest detectable beads is defined as the detection limit, which is $1.7 \times 10^{-6}$ mW, meaning that each single vesicle for which the SSC power was equal to or higher than $1.7 \times 10^{-6}$ mW would be detected.

Now the diameter of the smallest detectable single vesicles by flow cytometry can be assessed. Figure 5C is a close-up of the lower part of Fig. 5A, extended with the calculated FSC power of vesicles. Note that the vesicles scatter light less efficiently than beads, owing to their lower refractive index. As the exact refractive index of vesicles is unknown, the light green area represents an estimated confidence interval, which is based on an assumed inner refractive index of biological vesicles of $1.38 \pm 0.02$. Figure 5D is a close-up of the lower part of

Fig. 5B, extended with the calculated SSC power of vesicles. As the detection limit is $1.7 \times 10^{-6}$ mW, the estimated diameter range of the smallest detectable single vesicle is 300–700 nm, which contradicts our finding that vesicles smaller than 220 nm can be detected by flow cytometry (Fig. 3).

*Detection of vesicles smaller than 220-nm and 89-nm silica beads*

We hypothesize that the detection of vesicles smaller than 220 nm is a consequence of swarm detection; that is, multiple vesicles are simultaneously illuminated by the laser beam and counted as a single event signal. As a proof of principle, silica beads with a diameter of 89 nm, significantly below the 203 nm of single detectable beads, were prepared at a concentration of $10^{10}$ mL$^{-1}$ and successfully detected, as reflected by the SSC histogram shown in Fig. 6A. Thus, 89-nm beads with a refractive index close to that of vesicles can also be detected by flow cytometry at sufficiently high concentrations, owing to swarm detection.

*Single bead detection vs. swarm detection*

For polydisperse samples, such as vesicles in plasma and urine, it is interesting to know whether a count is generated by one
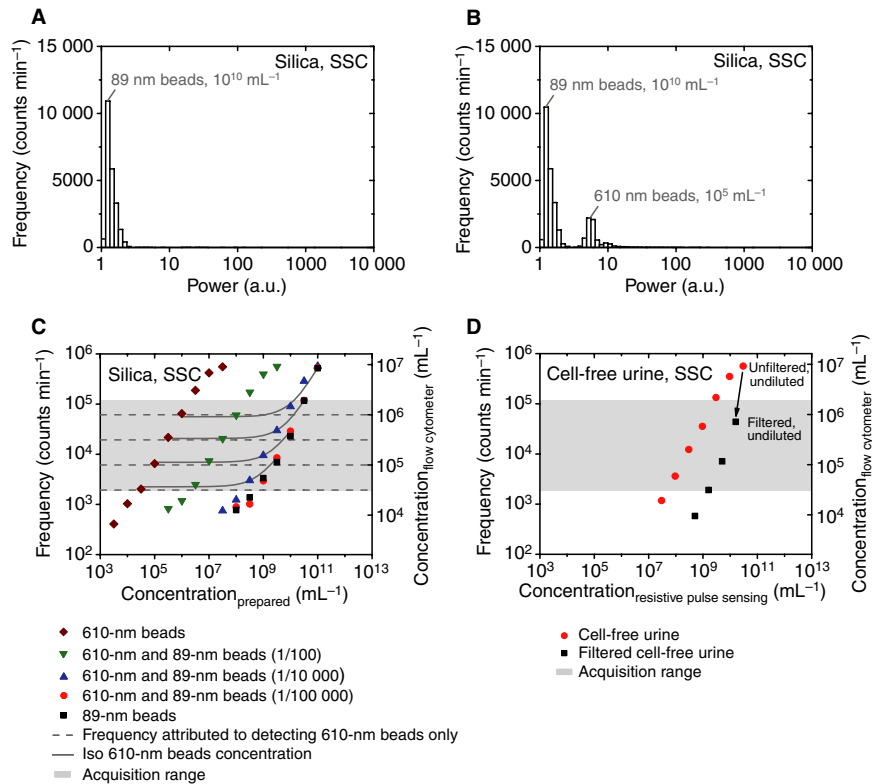
**Fig. 6.** Relative contributions of mechanisms underlying vesicle detection. Side-scattered light (SSC) histogram (logarithmic horizontal scale) for (A) 89-nm silica beads at a concentration of $1 \times 10^{10}$ mL$^{-1}$, and (B) a mixture of 89-nm and 610-nm silica beads at concentrations of $1 \times 10^{10}$ mL$^{-1}$ and $1 \times 10^5$ mL$^{-1}$, respectively. (C) Frequency or count rate vs. total concentration (logarithmic scales) of 610-nm silica beads (diamonds), 89-nm silica beads (squares), mixtures of 610-nm and 89-nm silica beads prepared at ratios of 1 : 100 (green triangles), 1 : 10 000 (blue triangles), and 1 : 100 000 (circles), and (D) cell-free urine and cell-free urine filtered (arrow) through a 220-nm filter. The right vertical axis shows the concentration as determined with the flow cytometer. Data points within the acquisition range (gray area) should be considered reliable. The error bars overlap with the symbols and are omitted to improve legibility. The dashed horizontal lines indicate the count rates corresponding to the detection of 610-nm silica beads at four different concentrations. The solid gray lines are exponential fits through data points with similar concentrations of 610-nm silica beads. a.u., arbitrary units.

large particle or by multiple small particles present in the laser beam. Here, a large or a small particle is defined as a particle scattering more or less light, respectively, than the detection limit of the flow cytometer. Consequently, the presence of one large particle or of multiple small particles in the laser beam will both be counted as a single event signal. Figure 6B shows the SSC histogram of a mixture of small 89-nm silica beads with a concentration of $10^{10}$ mL$^{-1}$ and large 610-nm silica beads with a concentration of $10^5$ mL$^{-1}$. The first peak is attributed to the high concentration of 89-nm beads, and the second peak is attributed to the $10^5$-fold lower concentration of 610-nm beads. Considering the low concentration of 610-nm beads as compared with that of the 89-nm beads, it is clear that the count rate is dominated by the large particles.

Dilution series are used to investigate the relative contributions of large and small particles to the count rate of the flow cytometer. Figure 6C shows the dilution curves of different ratios of 89-nm and 610-nm silica beads. The horizontal axis represents the sum of the prepared concentrations of 89-nm and 610-nm silica beads. The left vertical axis shows the count rate (frequency) as determined by the flow cytometer. As the flow rate was known, the concentration as determined by the

flow cytometer was also calculated, and is shown on the right vertical axis. First, with large 610-nm beads only, the flow cytometer-determined concentration obviously equaled that of the prepared concentration, and, within the acquisition range (gray area), the relationship between count rate and concentration was linear (dark red diamonds). Second, after addition of 100 beads of 89 nm to each 610-nm bead, the flow cytometer-determined concentration remained similar to that of the samples containing 610-nm beads only (dashed horizontal lines), meaning that, at this concentration, the 89-nm beads had no influence on the count rate (green triangles). Third, if we added 10 000 beads of 89 nm to each 610-nm bead, the flow cytometer-determined concentration increased by 40%, on average, in comparison with the samples containing 610-nm beads only (blue triangles), and with addition of 100 000 beads of 89 nm to each 610-nm bead, the flow cytometer-determined concentration increased by 350%, on average, in comparison with the samples containing 610-nm beads only (red circles). For the latter mixture, the relationship between count rate and prepared concentration is non-linear, as indicated by the increased slope, and the data overlap with those of the pure 89-nm beads (black squares), indicating that

the count rate is dominated by the simultaneous presence of multiple 89-nm beads in the laser beam.

*Single vesicle detection vs. swarm detection*

Figure 6D shows the dilution curves of cell-free urine and cell-free urine filtered through a 220-nm filter. With resistive pulse sensing (data not shown), the concentrations of vesicles in unfiltered and filtered cell-free urine were estimated to be $3.0 \times 10^{10}$ mL$^{-1}$ and $1.6 \times 10^{10}$ mL$^{-1}$, respectively. For cell-free urine, the relationship between the count rate and the concentration is linear, meaning that the counts are predominantly caused by single large vesicles. However, the dilution curve of the filtered cell-free urine reveals that small vesicles also contribute to the count rate (Fig. 6D). The relationship between count rate and concentration of filtered cell-free urine is non-linear, as indicated by the increased slope, confirming that the counts are caused by swarm detection.

## Discussion and conclusion

We have developed a model that relates the measured light scattering power to the diameter of single vesicles by combining measurements on polystyrene beads and silica beads with Mie calculations. Two mechanisms for vesicle detection by flow cytometry can be derived from the results. First, a single vesicle is counted if its diameter is larger than 300–700 nm, i.e. the smallest detectable single vesicle diameter estimated for our flow cytometer. Second, a swarm of multiple smaller vesicles is counted as a single event signal if the power of light scattered by all vesicles that are simultaneously present in the laser beam exceeds the detection limit. For polydisperse samples, such as vesicles in plasma and urine, counts are generated by a combination of single particle and swarm detection.

If large and small particles are defined as particles scattering more or less light than the detection limit of the flow cytometer, single particle detection is caused by large particles only. As every large particle is counted (Table 1), the concentration as determined by the flow cytometer equals the prepared concentration, and a linear relationship between count rate and prepared concentration is obtained, as demonstrated with the use of large 610-nm silica beads only (Fig. 6C).

Swarm detection, on the other hand, is caused by the detection of small particles only. As multiple small particles have to be simultaneously present in the laser beam to generate a single event signal, the flow cytometer-determined concentration underestimates the real concentration, and the relationship between count rate and prepared concentration is non-linear. Although the diameters of the smallest detectable single polystyrene and silica beads are 203 nm and 204 nm, respectively, we demonstrated that we could detect high concentrations of 89-nm silica beads (Fig. 6A) and vesicles filtered through a 220-nm filter (Fig. 3C,D), owing to swarm detection. For both samples, the flow cytometer-determined concentration is more than 1000-fold lower than the real concentration (Fig. 6C,D), and the relationship between count

rate and concentration is non-linear. As the detection limit of the flow cytometer is $1.7 \times 10^{-6}$ mW and the mean SSC powers of an 89-nm silica bead and a urinary vesicle are $2.2 \times 10^{-8}$ mW and $1.1 \times 10^{-8}$ mW, respectively, at least 77 silica beads or 155 vesicles have to be simultaneously present in the laser beam to generate a signal. For both samples, this requirement was fulfilled, as the estimated volume of the laser beam is 54 pL and the concentrations of silica beads and vesicles are $10^{10}$ mL$^{-1}$ and $1.6 \times 10^{10}$ mL$^{-1}$, respectively, so that, on average, 540 silica beads or 864 vesicles were simultaneously present in the beam. Figure 7 shows the dilution curves of 89-nm silica beads for high, medium and low flow rates. Within the acquisition range (gray area), the established concentration underestimates the prepared concentration, and the relationship between count rate and prepared concentration is non-linear. As a lower flow rate yields a smaller cross-sectional area of the sample stream and thus a smaller effective beam volume [28], a higher concentration of 89-nm silica beads is required to generate an event signal. Consequently, the dilution curves in Fig. 7 are shifted to the right with decreasing flow rates.

For samples containing a mixture of large and small particles, such as vesicles in plasma and urine, counts are generated by both single particle and swarm detection. If the concentration of small particles is lower than the threshold for generation of a signal, the count rate is dominated by large particles, and a linear relationship between count rate and concentration is obtained (Fig. 6C). However, if the concentration of small particles equals or exceeds the threshold for generation of a signal, the contribution of small and large particles to the count rate depends on the relative size and concentration of particles (Fig. 6C). For cell-free urine, we have shown that small vesicles contribute to the count rate by
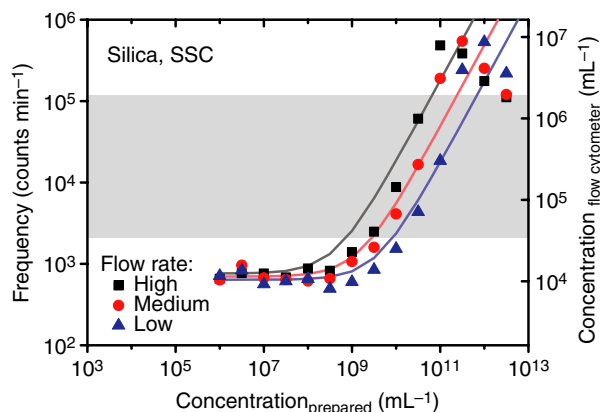


**Fig. 7.** Flow rate dependency of swarm detection. Frequency or count rate vs. total concentration (logarithmic scales) of 89-nm silica beads at high (63 μL min$^{-1}$; squares), medium (37 μL min$^{-1}$; circles) and low (12 μL min$^{-1}$; triangles) flow rates. The solid lines are linear fits through the data points below the maximum acquisition range. The right vertical axis shows the concentration as determined by the flow cytometer. Data points within the acquisition range (gray area) should be considered reliable. The error bars overlap with the symbols and are omitted to improve legibility. SSC, side-scattered light.

using a 220-nm filter. Without filtration, a fairly linear relationship between the count rate and the concentration is obtained, indicating that large vesicles, i.e. vesicles larger than 300–700 nm, are present. Vesicles larger than 295 nm were not observed by TEM imaging (Fig. 2), probably because the amount of imaged vesicles did not represent the full population, and because the diameter was affected by preanalytic factors, such as centrifugation, staining, fixation, and adhesion [29]. Note that the concentration as determined by the flow cytometer is 1000-fold lower than the concentration estimated with resistive pulse sensing, which was observed when flow cytometry was compared with other, novel detection methods [15,16]. The presence of multiple vesicles in the laser beam explains why the concentration is underestimated 1000-fold, but, more importantly, swarm detection allows the detection of smaller vesicles than previously thought possible.

### Sensitivity increases with collection angle

Although it is often thought that FSC should be used to determine the size of vesicles [8,9,11,30,31], Fig. 4A–D shows that, for our flow cytometer, the SSC detector is more sensitive and has a higher capability to resolve the size of beads than the FSC detector, as confirmed by other groups using instruments with a similar optical layout [28,30,32]. In this section, we will explain this phenomenon. Figure 8 shows the optical detection geometry of a flow cytometer (A) and how this affects the detection of light scattered by a cell (B), a microparticle (C), or an exosome (D). Each cell, microparticle or exosome is

illuminated by a laser beam with a constant intensity, which we estimate to be $1.4 \times 10^7$ W m$^{-2}$. The FSC detector is a photodiode that detects light which is scattered under an angle of approximately 0.5–7°, depending on the setup of the instrument. To prevent the laser directly illuminating the FSC detector, both the laser beam itself and the light scattered under an angle smaller than 0.5° are blocked by the so-called obscuration bar, as indicated by the interruption in the red line. The SSC detector is a photomultiplier tube, which is not only more sensitive than the photodiode of the FSC detector, but also detects scattered light over a much broader angle, i.e. 47–133°. The dashed blue lines inside the gray circular diagrams show how much light is scattered in each direction. Figure 8B shows that a cell with a diameter of 5 μm scatters light predominantly in the forward direction, which is in the direction of the FSC detector. Hence, FSC is associated with cell size. Figure 8C shows that a microparticle with a diameter of 500 nm scatters light differently than a cell, i.e. mainly under an angle of 0–10°. In comparison with the cell, the fraction of light scattered in the direction of the FSC detector has decreased, whereas the fraction of light scattered in the direction of the SSC detector has increased. Figure 8D shows that an exosome with a diameter of 50 nm scatters light nearly isotropically. As a result, more light is scattered in the direction of the SSC detector than in the direction of the FSC detector. As organelles are of a similar size as microparticles and exosomes, an increased SSC is commonly associated with the complex anatomy of cells. In fact, the SSC detector is optimized to detect scattering from multiple particles smaller than the
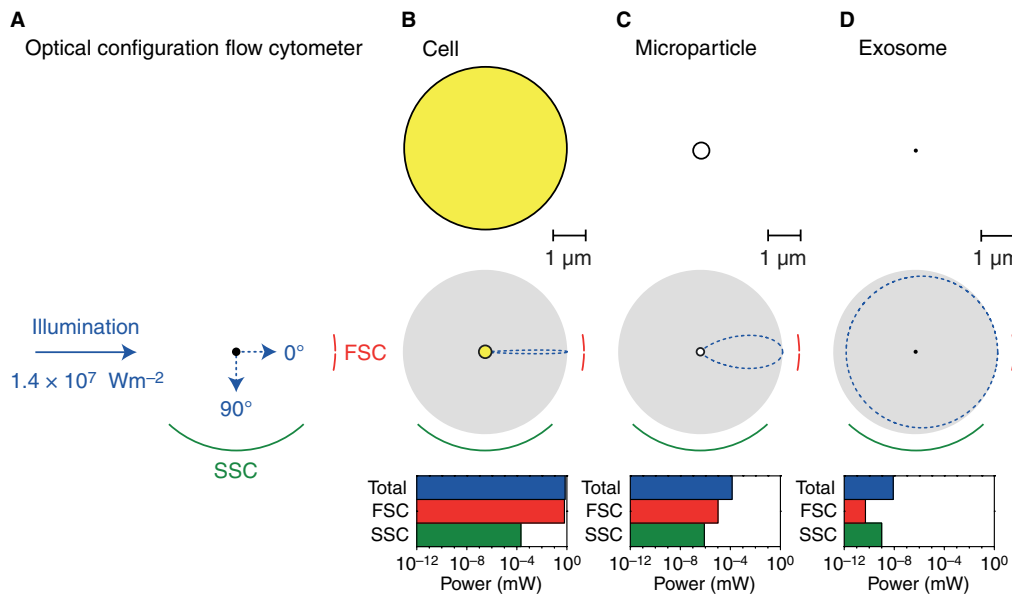


**Fig. 8.** Optical detection geometry of the FACSCalibur and the angular intensity distribution of light scattered by a single cell, a microparticle, or an exosome. (A) A particle (black dot) is illuminated by a laser beam (blue solid arrow). Forward-scattered light (FSC) and side-scatterered light (SSC) are collected between 0.5° and 7° (red lines) and between 47° and 133° (green line), respectively. The gray circular diagrams show the angular intensity distribution (blue dashed line) of perpendicularly polarized light scattered by a cell (yellow circle) with diameter 5 μm (B), a microparticle (white circle) with diameter 500 nm, and an exosome (black dot) with diameter 50 nm (C). The scattering angle becomes wider for decreasing cell or vesicle diameters. The bar plots at the bottom show the power (logarithmic scale) scattered in all directions (blue), the power scattered in the FSC direction (red), and the power scattered in the SSC direction (green). The calculation parameters are listed in Table 2.

wavelength. Thus, to increase the sensitivity for vesicle detection, it is beneficial to select the detector with the largest collection angle. For most regular flow cytometers, this implies using the SSC detector.

### Implications and limitations

Our model explains several recent observations regarding vesicle detection with flow cytometry. In an effort to standardize vesicle detection, the ISTH Scientific Standardization Committee proposed a protocol that used 500-nm and 900-nm polystyrene beads from Megamix to define a vesicle size gate [8]. They observed that flow cytometer-determined concentrations of vesicles appeared to be consistent among instruments measuring FSC with a relatively wide solid angle (1–19°; Beckman-Coulter), but appeared to be inconsistent among instruments measuring FSC with a low solid angle (0.7–10°; Becton-Dickinson). The low collection angle makes the detection limit strongly dependent on the width of the obscuration bar, which is specific for each individual instrument. As vesicle detection typically takes place near the detection limit, the results differed among the Becton-Dickinson instruments.

Chandler et al. applied the Megamix gating strategy to detect platelet microparticles (PMPs) on the Apogee A40, which has an FSC collection angle of 1–70°, and showed that mainly platelets, which have an average diameter of 2000–5000 nm [33], were counted [9]. Unlike Chandler et al., Mullier et al. and Robert et al. [10,11] could perfectly distinguish PMPs from platelets by using the same gating strategy on their flow cytometers, which all had an FSC collection angle below 19°. To explain this discrepancy and to show that our calibration procedure is generally applicable, we have determined the calibration factors for the FSC detectors of the Apogee A40 and the Beckman-Coulter FC500 by using their data [9,11]. Figure 9A,B shows the diameters of single vesicles as selected by the Megamix gating strategy for the Apogee A40 and FC500, respectively. The range of diameters of single vesicles gated on the Apogee A40 is 200 nm larger than the range gated on the FC500. Owing to the wider collection angle of the Apogee A40 than of the FC500, the Apogee A40 is more sensitive to the difference in refractive index between polystyrene beads and vesicles than the FC500. Nevertheless, single PMPs are not expected to appear in the gated range for either the Apogee A40 or the FC500, as the measured PMP diameter is far below 500 nm [15,16,32]. Rather, it is the presence of multiple PMPs in the laser beam that makes them detectable by flow cytometry. From reference measurements with novel methods, we know that the concentration of PMPs exceeds $10^{10}$ mL$^{-1}$ [32], which ensures that multiple vesicles are illuminated simultaneously and is sufficient to generate a single event signal.

For functional research on vesicles, the presence of multiple vesicles in the beam may have major consequences. For example, different fluorescence signals corresponding to a 'single event signal' may originate from multiple vesicles, each containing a different antibody, which may explain the colocalization of granulocyte (CD66e) and platelet (CD61) markers on tissue factor-exposing vesicles [34]. On the other hand, as all vesicles contribute to the signal, our findings explain why flow cytometry results often correlate with disease.

Our work may lead to a better understanding of vesicle detection by flow cytometry, increased sensitivity by optimizing the instrument-specific settings, and improvements in the standardization of measurements between laboratories, which involves at least four steps. First, the scattering power of beads should be measured for the detector with the largest collection angle and highest sensitivity. Second, the scattering power of beads should be calculated specifically for the used detector by Mie theory. Third, the calibration factor should be determined to quantify the detection signal. Fourth, a gate should be selected on the basis of the quantified optical power. For
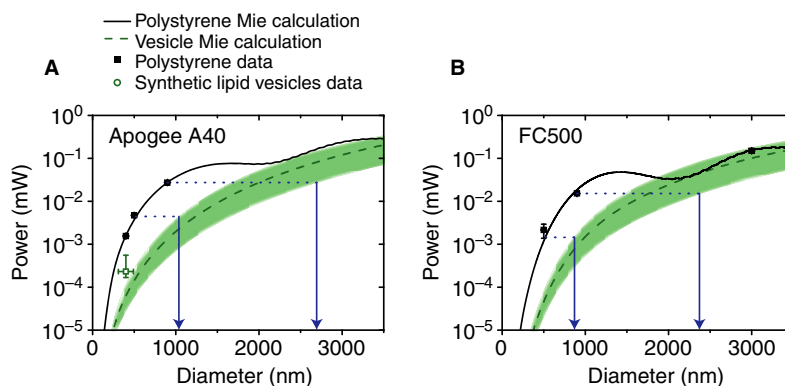


**Fig. 9.** Selected vesicle diameter range obtained by applying the Megamix gating strategy on the Apogee A40 vs. the FC500. (A) Measured (symbols) and calculated (lines) forward-scattered light (FSC) power (logarithmic scale) vs. diameter for polystyrene beads (black) and vesicles (circle), for the Apogee A40. The measured data points are adopted from Chandler et al. [9]. The obtained calibration factor is $2.67 \times 10^{-6}$. The Megamix gating strategy would select single vesicles with a diameter between 1000 nm and 2700 nm. (B) Measured and calculated FSC power vs. diameter for polystyrene beads and vesicles for the FC500. The measured data points are adopted from Robert et al. [11]. The obtained calibration factor is $5.18 \times 10^{-4}$. The Megamix gating strategy would select single vesicles with a diameter between 800 nm and 2400 nm. The calculation parameters are listed in Table 2.

improved standardization, the relationship between the detected scattering power from multiple vesicles, the volume of the laser beam and the flow rate requires further investigation. For improved vesicle detection, we suggest modification of the hardware of the flow cytometer [35], and study of the refractive index of vesicles and the medium. In addition, as many studies also use fluorescence to identify vesicles, we suggest performing a detailed analysis on fluorescent beads, although many non-trivial practical and theoretical problems will have to be solved before a comparable study based on fluorescence can be performed [7]. In spite of its limitations, flow cytometry will still have to be the present method of choice, because we do not yet have validated methods for quantitative enumeration and establishment of the cellular source of vesicles.

In conclusion, we have established a model that relates the detected scattering power to the diameter of single vesicles. The gating strategy proposed by the Scientific Standardization Committee collaborative workshop selects single vesicles and cells with diameters between 800 nm and 2400 nm when applied on the FSC detector of regular flow cytometers. However, vesicle detection by regular flow cytometry is relies on two different mechanisms: (i) detection of single, relatively large, vesicles that scatter more light than the detection limit; and (ii) swarm detection – that is, multiple relatively small vesicles are simultaneously illuminated by the laser beam and counted as a single event signal. Swarm detection allows the detection of smaller vesicles than previously thought possible. It explains the finding that flow cytometry underestimates the concentration of vesicles, and it clarifies several observations published by the ISTH Scientific Standardization Committee collaborative workshop on vesicle detection.

## Acknowledgements

## Disclosure of Conflict of Interests

The authors state that they have no conflict of interest.

## References

1 Simons M, Raposo G. Exosomes – vesicular carriers for intercellular communication. *Curr Opin Cell Biol* 2009; **21**: 575–81.

2 Nieuwland R, Sturk A. Why do cells release vesicles? *Thromb Res* 2010; **125**: S49–51.

3 Ratajczak J, Wysoczynski M, Hayek F, Janowska-Wieczorek A, Ratajczak MZ. Membrane-derived microvesicles: important and under-appreciated mediators of cell-to-cell communication. *Leukemia* 2006; **20**: 1487–95.

4 Berckmans RJ, Sturk A, Schaap MC, Nieuwland R. Cell-derived vesicles exposing coagulant tissue factor in saliva. *Blood* 2011; **117**: 3172–80.

5 Manly DA, Wang JG, Glover SL, Kasthuri R, Liebman HA, Key NS, Mackman N. Increased microparticle tissue factor activity in cancer patients with venous thromboembolism. *Thromb Res* 2010; **125**: 511–12.

6 Rautou PE, Leroyer AS, Ramkhelawon B, Devue C, Duflaut D, Vion AC, Nalbone G, Castier Y, Leseche G, Lehoux S, Tedgui A, Boulanger CM. Microparticles from human atherosclerotic plaques promote endothelial ICAM-1-dependent monocyte adhesion and transendothelial migration. *Circ Res* 2011; **108**: 335–43.

7 van der Pol E, Hoekstra AG, Sturk A, Otto C, van Leeuwen TG, Nieuwland R. Optical and non-optical methods for detection and characterization of microparticles and exosomes. *J Thromb Haemost* 2010; **8**: 2596–607.

8 Lacroix R, Robert S, Poncelet P, Kasthuri RS, Key NS, Dignat-George F. Standardization of platelet-derived microparticle enumeration by flow cytometry with calibrated beads: results of the International Society on Thrombosis and Haemostasis SSC Collaborative workshop. *J Thromb Haemost* 2010; **8**: 2571–4.

9 Chandler WL, Yeung W, Tait JF. A new microparticle size calibration standard for use in measuring smaller microparticles using a new flow cytometer. *J Thromb Haemost* 2011; **9**: 1216–24.

10 Mullier F, Bailly N, Chatelain C, Dogné JM, Chatelain B. More on: calibration for the measurement of microparticles: needs, interests, and limitations of calibrated polystyrene beads for flow cytometry-based quantification of biological microparticles. *J Thromb Haemost* 2011; **9**: 1679–81.

11 Robert S, Poncelet P, Lacroix R, Raoult D, Dignat-George F. More on: calibration for the measurement of microparticles: value of calibrated polystyrene beads for flow cytometry-based sizing of biological microparticles. *J Thromb Haemost* 2011; **9**: 1676–8.

12 Robert S, Poncelet P, Lacroix R, Arnaud L, Giraudo L, Hauchard A, Sampol J, Dignat-George F. Standardization of platelet-derived microparticle counting using calibrated beads and a Cytomics FC500 routine flow cytometer: a first step towards multicenter studies? *J Thromb Haemost* 2009; **7**: 190–7.

13 Perez-Pujol S, Marker PH, Key NS. Platelet microparticles are heterogeneous and highly dependent on the activation mechanism: studies using a new digital flow cytometer. *Cytometry A* 2007; **71**: 38–45.

14 Welton JL, Khanna S, Giles PJ, Brennan P, Brewis IA, Staffurth J, Mason MD, Clayton A. Proteomics analysis of bladder cancer exosomes. *Mol Cell Proteomics* 2010; **9**: 1324–38.

15 Yuana Y, Oosterkamp TH, Bahatyrova S, Ashcroft B, Garcia RP, Bertina RM, Osanto S. Atomic force microscopy: a novel approach to the detection of nanosized blood microparticles. *J Thromb Haemost* 2010; **8**: 315–23.

16 Harrison P, Dragovic R, Albanyan A, Lawrie AS, Murphy M, Sargent I. Application of dynamic light scattering to the measurement of microparticles. *J Thromb Haemost* 2009; **7**(Suppl. 2): OC-TU-056.

17 van Manen HJ, Verkuijlen P, Wittendorp P, Subramaniam V, van den Berg TK, Roos D, Otto C. Refractive index sensing of green fluorescent proteins in living cells using fluorescence lifetime imaging microscopy. *Biophys J* 2008; **94**: L67–9.

18 Beuthan J, Minet O, Helfmann J, Herrig M, Muller G. The spatial variation of the refractive index in biological cells. *Phys Med Biol* 1996; **41**: 369–82.

19 Foladori P, Quaranta A, Ziglio G. Use of silica microspheres having refractive index similar to bacteria for conversion of flow cytometric forward light scatter into biovolume. *Water Res* 2008; **42**: 3757–66.

20 Briggs C, Harrison P, Samuel JM. Platelet counting. In: Michelson AD, ed. *Platelets*, 2nd edn. San Diego, CA: Academic Press, 2006: 475–83.

21 Collier JL. Flow cytometry and the single cell in phycology. *J Phycol* 2000; **36**: 628–44.

22 Goddard G, Martin JC, Naivar M, Goodwin PM, Graves SW, Habbersett R, Nolan JP, Jett JH. Single particle high resolution spectral analysis flow cytometry. *Cytometry A* 2006; **69**: 842–51.

23 Snow C. Flow cytometer electronics. *Cytometry A* 2004; **57**: 63–9.

24 Bohren CF, Huffman DR. *Absorption and Scattering of Light by Small Particles*. New York, NY: Wiley, 1983.

25 Mätzler C. MATLAB functions for Mie scattering and absorption. 2002–11. Bern, Institute of Applied Physics: University of Bern, 2002.

26 Fattaccioli J, Baudry J, Emerard JD, Bertrand E, Goubault C, Henry N, Bibette J. Size and fluorescence measurements of individual droplets by flow cytometry. *Soft Matter* 2009; **5**: 2232–8.

27 Laven P. MIEPLOT. http://www.philiplaven.com. Accessed 21 November 2011.

28 Shapiro HM, Leif RC. *Practical Flow Cytometry*, 4th edn. NJ: Wiley, 2003.

29 Yuana Y, Bertina RM, Osanto S. Pre-analytical and analytical issues in the analysis of blood microparticles. *Thromb Haemost* 2011; **105**: 396–408.

30 Tocchetti EV, Flower RL, Lloyd JV. Assessment of in vitro-generated platelet microparticles using a modified flow cytometric strategy. *Thromb Res* 2001; **103**: 47–55.

31 Lacroix R, Robert S, Poncelet P, Dignat-George F. Overcoming limitations of microparticle measurement by flow cytometry. *Semin Thromb Hemost* 2010; **36**: 807–18.

32 Dragovic RA, Gardiner C, Brooks AS, Tannetta DS, Ferguson DJ, Hole P, Carr B, Redman CW, Harris AL, Dobson PJ, Harrison P, Sargent IL. Sizing and phenotyping of cellular vesicles using nano-particle tracking analysis. *Nanomedicine* 2011; **7**: 780–8.

33 White JG. Platelet structure. In: Michelson AD, ed. *Platelets*, 2nd edn. San Diego, CA: Academic Press, 2006: 45–73.

34 Diamant M, Nieuwland R, Pablo RF, Sturk A, Smit JW, Radder JK. Elevated numbers of tissue-factor exposing microparticles correlate with components of the metabolic syndrome in uncomplicated type 2 diabetes mellitus. *Circulation* 2002; **106**: 2442–7.

35 Steen HB. Flow cytometer for measurement of the light scattering of viral and other submicroscopic particles. *Cytometry A* 2004; **57**: 94–9.